Catal Lett (2008) 120:126–136
DOI 10.1007/s10562-007-9263-x

Preparation, Characterization and Catalytic Activity of Palladium Nanoparticles Encapsulated in SBA-15

Changli Li · Qinghong Zhang · Ye Wang · Huilin Wan

Received: 12 August 2007 / Accepted: 30 August 2007 / Published online: 15 September 2007

Abstract A simple adsorption method was studied for the preparation of SBA-15-encapsulated palladium nanoparticles. This method employed the SBA-15 with organic template removed by ethanol extraction for the adsorption of cationic Pd precursors in alkaline solution followed by calcination and H_2 reduction. The pH of the solution was found to be a critical factor in determining the palladium content and the ordered mesoporous structure. Our characterizations revealed that the Pd nanoparticles prepared by this method were located inside the mesoporous channels and were quite uniform in size (mostly 3–4 nm). The SBA-15-encapsulated uniform Pd nanoparticles were efficient catalysts for solvent-free aerobic oxidation of alcohols.

Keywords Palladium nanoparticles · SBA-15 · Adsorption method · Alcohol oxidation

1 Introduction

Palladium catalysts are playing essential roles in many important organic transformations such as hydrogenation, Heck and Suzuki couplings and aerobic oxidation of alcohols [1–4]. Recent studies have suggested that Pd nanoparticles may function as active species in these organic reactions. Particularly, recent reports have revealed that supported Pd nanoparticles show promising catalytic performances for the aerobic oxidation of alcohols even under solvent-free conditions, which is an important transformation from the viewpoints of establishing a green process for the synthesis of carbonyl compounds to replace the conventional stoichiometric oxidation process using dichromate or permanganate. For example, Pd nanoparticles generated on the hydroxyapatite during the aerobic oxidation of 1-phenylethanol were found to be the true active species, and the hydroxyapatite-supported Pd nanoparticles with a mean size of 3.8 nm were more active that those with a mean size of 7.8 nm for the oxidation of 1-phenylethanol or benzhydrol [4]. Pd nanoparticles supported on magnesia or entrapped in aluminum hydroxide were also efficient catalysts for the aerobic oxidation of alcohols [5, 6]. We reported that the highly dispersed Pd(II) species adsorbed on Al_2O_3 were transformed into Pd nanoparticles with a mean size of $\sim$5 nm during the course of aerobic oxidation of benzyl alcohol, and the generated Pd nanoparticles accounted for the solvent-free aerobic oxidation of benzyl alcohol [7]. Under such background, the controllable synthesis of Pd nanoparticles with tunable and uniform sizes would be helpful for the design of efficient heterogeneous catalysts for these important organic reactions.

Because of the large surface areas and ordered size-tunable porous channels, mesoporous materials have received great interests for the synthesis of metal nanoparticles with narrow size distributions [8–11]. Several pathways are known for incorporating metal nanoparticles into mesoporous silica. The most conventional method was impregnation of mesoporous silica with metal precursor solution followed by thermal treatment and reduction with H_2. Sonication-aided impregnation [12, 13] and chemical vapor deposition [14] were also exploited for the preparation of metal nanoparticles in mesoporous silica. Somorjai and coworkers [15, 16] developed an effective two-step method for the synthesis of metal nanoparticles (especially Pt)

C. Li · Q. Zhang (✉) · Y. Wang · H. Wan
State Key Laboratory of Physical Chemistry of Solid Surfaces and Department of Chemistry, College of Chemistry and Chemical Engineering, Xiamen University, Xiamen 361005, China
e-mail: zhangqh@xmu.edu.cn

encapsulated in SBA-15 by hydrothermal growth of mesoporous silica (SBA-15) in the presence of pre-prepared polymer-stabilized metal nanoparticles.

As far as the SBA-15-incorporated palladium nanoparticles are concerned, the studies are quite limited. The simple impregnation has been employed for the preparation of SBA-15-supported Pd particles [17, 18], but this method could not ensure the encapsulation of Pd nanoparticles inside the mesoporous channels. Chemical vapor infiltration was once used for the preparation of SBA-15-confined Pd [19], but Pd nanowires were mainly obtained. Yuranov et al. [20, 21] reported interesting work on the preparation of Pd nanoparticles confined in the mesopores or the complementary micropores of SBA-15 via an ion exchange procedure.

We have recently studied the preparation and the catalytic activity of Pd nanoparticles encapsulated in mesoporous channels of SBA-15 for the aerobic oxidation of alcohols under solvent-free conditions. It is well known that the oxide surface may be charged in aqueous solution, and the charge nature of the surface depends on the pH of the solution and the point of zero charge (PZC) of the support, defined as the pH value where the surface charge is zero [22]. The electrostatic adsorption of metal precursors onto the inversely charged support surface would occur by properly regulating the pH of the aqueous solution containing metal precursors. This method has been used for the preparation of supported metal or metal oxide catalysts with high dispersion of active components [22]. We reported in the previous paper [7] that Al_2O_3-supported highly dispersed Pd(II) species could be obtained by adsorption of $PdCl_4^{2-}$ onto Al_2O_3 under acidic conditions, where the Al_2O_3 surface was positively charged, and that the reduction of the highly dispersed Pd(II) species led to the formation of Pd nanoparticles of $\sim$5 nm on Al_2O_3. Using similar adsorption method, we recently succeeded in preparing SBA-15-encapsulated Pd nanoparticles. Here, we report our characterizations of the Pd/SBA-15 catalysts prepared by adsorption of $[Pd(NH_3)_4]^{2+}$ into SBA-15 under basic conditions followed by calcination and H_2 reduction. The catalytic results obtained for thus prepared Pd/SBA-15 catalysts in the solvent-free aerobic oxidation of alcohols are also discussed.

2 Experimental

2.1 Synthesis of SBA-15

SBA-15 was synthesized according to the procedures reported previously [23]. A Pluronic P123 triblock copolymer ($EO_{20}PO_{70}EO_{20}$) and tetraethyl orthosilicate (TEOS) were used as the organic template and the silica source, respectively. A homogeneous mixture containing $EO_{20}PO_{70}EO_{20}$ and TEOS in hydrochloric acid solution was first stirred in a round flask at 40 °C for 20 h. Then the resultant gel was transferred to a Teflon bottle, which was placed in a stainless-steel autoclave. After hydrothermal treatment at 100 °C for 24 h, the solid product was recovered by filtration, followed by washing with deionized water and drying at 50 °C in vacuum. In order to create hydroxyl groups with a high concentration for the adsorption in alkaline solution, we removed the organic template by solvent extraction because the removal of the organic template by calcination would deplete the surfaces of hydroxyl groups [20, 24]. Thus, the as-synthesized SBA-15 was placed in an excess amount of ethanol (1 g SBA-15/150 mL ethanol) and the mixture was stirred vigorously for 1 h at 45 °C followed by filtration to recover powdery SBA-15. After being treated with ethanol for three times, the finally recovered SBA-15 powder was dried overnight at 120 °C.

2.2 Preparation of Pd/SBA-15

The Pd/SBA-15 catalysts were prepared by adsorption of the Pd precursor, i.e., $[Pd(NH_3)_4]^{2+}$ onto the channel surface of SBA-15 followed by calcination and H_2 reduction. Typically, the SBA-15 (1 g) with organic template removed by ethanol extraction was added to the aqueous solution of $Pd(NH_3)_4Cl_2$ (50 mL) with a certain concentration (1.2–12.5 mmol L^{-1}). The pH of the solution was regulated to 8.3–11.0 by the addition of 5% ammonium hydroxide aqueous solution. Because the PZC of silica is ca. 3 [25], the surface silanol groups are expected to be converted to $\equiv Si–O^-$, and the adsorption of $[Pd(NH_3)_4]^{2+}$ via coulombic interactions can occur. After the mixture was stirred at room temperature for 4 h, the resultant solid was recovered by filtration and washing thoroughly with deionized water to remove all the unattached $[Pd(NH_3)_4]^{2+}$ and the Cl^-. The sample was then dried and calcined in air at 550 °C for 6 h, followed by reduction with H_2 at 300 °C. For comparison, the conventional impregnation was also applied to the preparation of Pd/SBA-15. In this case, SBA-15 with organic template removed by calcination at 550 °C in air was used for impregnation of $Pd(NH_3)_4Cl_2$ aqueous solution under a similar pH environment. After impregnation and drying, the sample was also subjected to calcination at 550 °C in air and reduction with H_2 at 300 °C. The sample prepared with this procedure was denoted as Pd/SBA-15-*imp*.

2.3 Characterization of Pd/SBA-15

Powder X-ray diffraction (XRD), N_2 sorption and transmission electron microscopy (TEM) measurements

were used to characterize the ordered mesoporous structures of the Pd/SBA-15 samples. TEM was also employed to evaluate the size of Pd nanoparticles. The dispersion of Pd was estimated by CO chemisorption. Diffuse reflectance UV–vis spectroscopy was performed to investigate the state of the palladium species before reduction.

XRD patterns were recorded on a Panalytical X'Pert Pro Super X-ray diffractometer equipped with X'Celerator and Xe detection systems. Cu-K_α radiation (40 kV and 30 mA) was used as the X-ray source. N_2 sorption at 77 K was carried out with a Micromeritics Tristar 3000 surface and porosimetry analyzer. The surface area, pore volume and pore size distribution were evaluated by the BET and BJH methods. TEM measurements were performed on a Tecnai F30 electron microscope (Phillips Analytical) operated at an acceleration voltage of 300 kV. Samples for TEM measurements were suspended in ethanol and dispersed ultrasonically. Drops of the suspensions were applied on a copper grid coated with carbon. The size distribution of Pd particles was determined from the TEM images by surveying more than 100 Pd particles. CO chemisorption was carried out with a Micromeritics ASAP 2010C. Before the introduction of CO, the sample was pretreated by O_2-containing gas flow at 450 °C for 1 h followed by reduction with H_2 at 300 °C for 1 h and then evacuated. CO chemisorption was measured at 35 °C. After the first isotherm (total CO uptake), the sample was evacuated for ~10 min, and the second isotherm (reversible CO uptake) was measured. The amount of the chemisorbed CO (irreversible CO uptake) was calculated using the difference between the total and reversible CO uptakes. The dispersion of Pd was estimated by assuming the stoichiometric molar ratio of (chemisorbed CO)/Pd = 1/1. Diffuse reflectance UV–vis spectra were recorded on a Varian Cary-5000 spectrometer equipped with a diffuse-reflectance accessory. The spectra were collected at 200–800 nm with $BaSO_4$ as a reference.

2.4 Catalytic Reaction

The solvent-free aerobic oxidation of alcohols was carried out using a batch-type reaction vessel with a reflux condenser. The typical reaction procedures were as follows. After the catalyst (0.1 g) was added into the alcohol (~50 mmol) placed in the reaction vessel, the mixture was heated to the reaction temperature with vigorous stirring. Then, the O_2 flow (3 mL min^{-1}) was bubbled into the mixture to start the reaction. After the reaction, the solid catalyst was filtered off and the liquid product was analyzed by GC after the addition of an internal standard.

3 Results and Discussion

3.1 Structure Features of the Pd/SBA-15

As described above, the surface of oxides may become positively or negatively charged depending on the pH value of the aqueous solution, where the oxide is placed [22, 25]. For silica, at a pH > PZC (ca. 3), the surface silanol groups could be transformed to $\equiv$Si–O^- (reaction 1) and the adsorption of $[Pd(NH_3)_4]^{2+}$ would occur. It is expected that the concentration of the $\equiv$Si–O^- sites depends on the pH value of the solution of Pd precursors (see Eqs. 2 and 3).

$$\equiv \mathrm{SiOH} + \mathrm{OH}^- \rightarrow \equiv \mathrm{SiO}^- + \mathrm{H_2O} \quad (1)$$

$$\equiv \mathrm{SiOH} \overset{K_a}{\leftrightarrows} \equiv \mathrm{SiO}^- + \mathrm{H}^+ \quad (2)$$

$$[\equiv \mathrm{SiO}] = K_a[\equiv \mathrm{SiOH}][\mathrm{OH}^-]/K_w \quad (3)$$

Therefore, the pH value of the aqueous solution of $[Pd(NH_3)_4]^{2+}$ would affect the Pd content introduced into SBA-15 by the adsorption method.

We regulated the pH value by changing the amount of ammonium hydroxide solution, and confirmed that almost no Pd could be incorporated into SBA-15 if the pH value was kept below 8. Table 1 shows the dependence of Pd content incorporated into SBA-15 on the pH value at different concentrations of $[Pd(NH_3)_4]^{2+}$. At a lower concentration of $[Pd(NH_3)_4]^{2+}$ (1.2 mmol L^{-1}), ca. 40% of Pd precursors in the solution were incorporated into the SBA-15 at a pH of 8.3. The increase in the $[Pd(NH_3)_4]^{2+}$ concentration increased the Pd content at a similar pH value, but the efficiency of Pd incorporation decreased.

Table 1 Effect of pH of the Pd precursor solutions on Pd content incorporated in the final Pd/SBA-15 samples[a]

$[Pd(NH_3)_4]^{2+}$ conc. (mmol L^{-1})	Pd content expected (wt%)	pH	Pd content in final sample[b] (wt%)
1.2	1.0	8.3	0.40
2.5	1.9	8.5	0.70
2.5	1.9	10.3	1.4
5.0	3.8	8.9	1.3
5.0	3.8	10.0	1.4
5.0	3.8	10.3	1.9
5.0	3.8	10.6	2.2
5.0	3.8	11.0	3.7
12.5	9.1	10.0	2.0
12.5	9.1	10.4	3.0
12.5	9.1	10.8	3.9

[a] SBA-15 after removal of organic template by ethanol extraction, 1 g; volume of aqueous solution of $[Pd(NH_3)_4]^{2+}$, 50 mL

[b] Detected by ICP measurements

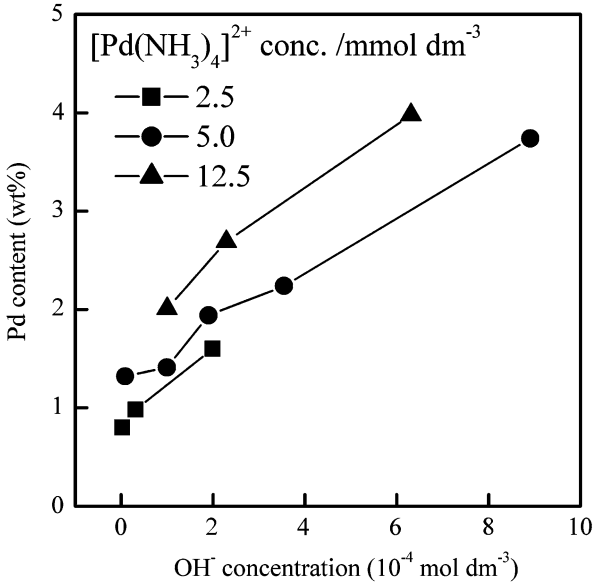

Fig. 1 Effect of the OH^- concentration of the aqueous solution of Pd precursors on the Pd content incorporated into SBA-15

Table 1 shows that the increase in pH value (or $[OH^-]$) at a fixed concentration of $[Pd(NH_3)_4]^{2+}$ could significantly increase the Pd content. The effect of the $[OH^-]$ on the Pd content incorporated into SBA-15 at different concentrations of $[Pd(NH_3)_4]^{2+}$ is further summarized in Fig. 1. In each case, the Pd content rose almost linearly with the $[OH^-]$, confirming that the reaction (1) and the adsorption of $[Pd(NH_3)_4]^{2+}$ on the $\equiv Si–O^-$ sites did occur. It should be noted that, as the pH value increased to ≥11.0, the ordered mesoporous structure of SBA-15 could not be sustained. Our results suggest that the highest content of Pd incorporated into SBA-15 is ~4 wt% using the present adsorption method.

Figures 2 and 3 show the XRD patterns of the Pd/SBA-15 samples at low and high diffraction angles, respectively. SBA-15 before or after calcination showed three diffraction peaks at 2θ degrees of 0.8–3° indexed to (100), (110) and (200) of the regularity of hexagonal array of mesopores of SBA-15. These peaks could still be clearly observed after the incorporation of Pd by the adsorption method although their intensities decreased to some extent. We speculate that such decreases may reflect the occupation of the mesoporous channels by Pd nanoparticles. The use of the alkaline medium for adsorption may also affect the long-range regularity of mesoporous array of these samples. Figure 3 shows that, at high diffraction angles (10–70°), the Pd/SBA-15 samples with Pd content <1.3 wt% showed only a broad diffraction peak at 2θ degree of ca. 23° ascribed to the amorphous framework of SBA-15. As Pd content exceeded 1.3 wt%, a weak and broad diffraction peak (2θ = ~40°) assignable to metallic Pd appeared. For comparison, the diffraction patterns at low and high diffraction angles for

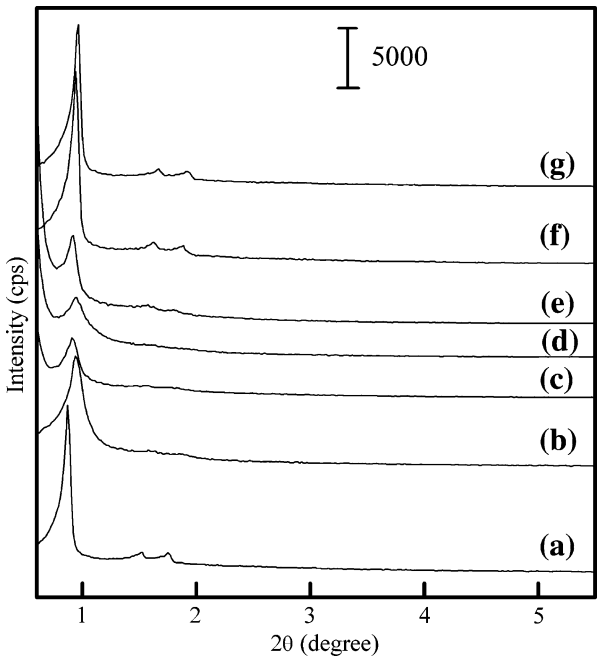

Fig. 2 XRD patterns at low diffraction angles. (a) SBA-15 without calcination, (b) 0.40 wt% Pd/SBA-15, (c) 0.70 wt% Pd/SBA-15, (d) 1.3 wt% Pd/SBA-15, (e) 2.0 wt% Pd/SBA-15, (f) SBA-15 calcined, (g) 0.41 wt% Pd/SBA-15-*imp*

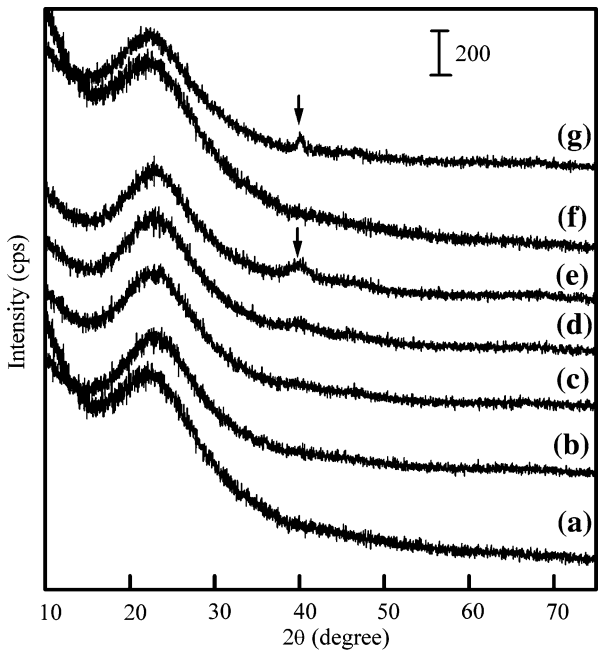

Fig. 3 XRD patterns at high diffraction angles. (a) SBA-15 without calcination, (b) 0.40 wt% Pd/SBA-15, (c) 0.70 wt% Pd/SBA-15, (d) 1.3 wt% Pd/SBA-15, (e) 2.0 wt% Pd/SBA-15, (f) SBA-15 calcined, (g) 0.41 wt% Pd/SBA-15-*imp*

the 0.41 wt% Pd/SBA-15-*imp* sample were also shown in Figs. 2 and 3, respectively. As shown in Fig. 2, the decrease in the long-range regularity of mesoporous structure after

the introduction of Pd to SBA-15 by the impregnation was less serious. A relatively sharp diffraction peak at 2θ degree of ~40° assignable to metallic Pd was already observed for this sample although the Pd content was only 0.41 wt%. This suggests that relatively larger Pd particles were formed in the Pd/SBA-15-*imp* sample. These Pd particles may not be located inside the mesoporous channels and thus have little effect on the ordered porous structure as shown in Fig. 2.

N_2 adsorption–desorption isotherms for the Pd/SBA-15 samples are shown in Fig. 4. SBA-15 exhibited the type-IV isotherms with a regular type-H1 hysteresis loop at relative pressures (p/p_0) of 0.7–0.75 due to the N_2 capillary condensation in cylindrical mesoporous channels [23]. As listed in Table 2, the BET surface area and pore volume of SBA-15 were 739 $m^2\ g^{-1}$ and 0.86 $cm^3\ g^{-1}$, respectively.

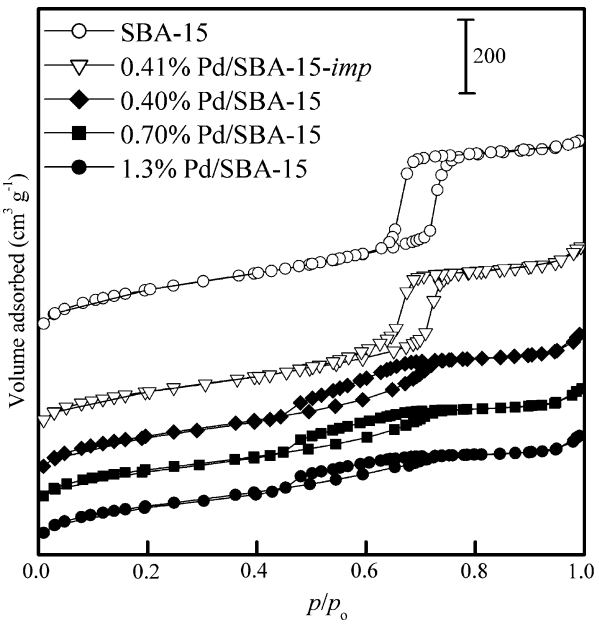

Fig. 4 N_2 adsorption–desorption isotherms for Pd/SBA-15 samples with different Pd contents as well as SBA-15

Table 2 Surface areas and porous parameters of Pd/SBA-15 samples

Sample	Surface area ($m^2\ g^{-1}$)	Average pore diameter (nm)	Pore volume ($cm^3\ g^{-1}$)
SBA-15	739	5.6	0.86
0.40 wt% Pd/SBA-15	724	4.7	0.66
0.70 wt% Pd/SBA-15	639	4.6	0.55
1.3 wt% Pd/SBA-15	643	4.4	0.49
2.2 wt% Pd/SBA-15	604	4.4	0.49
0.41 wt% Pd/SBA-15-*imp*	632	5.8	0.82

The pore size distribution evaluated from the desorption branch by the BJH method showed a maximum at ~6.0 nm (Fig. 5A), and the calculation gave an average pore diameter of 5.6 nm for SBA-15. These features were consistent with those reported previously [23]. Similar N_2-sorption isotherms and pore size distribution curve were obtained for the 0.41 wt% Pd/SBA-15-*imp* sample. The surface area and the pore volume for this sample became slightly lower than those for SBA-15 alone (Table 2). On the other hand, for the Pd/SBA-15 series of samples prepared by the adsorption method, although the type-IV isotherms still remained, the pattern of hysteresis loop changed markedly. As shown in Fig. 4, wider hysteresis loops at p/p_0 of 0.45–0.70 were observed for these samples, and such wide hysteresis loops were characteristic of the percolation effect [26], which could be explained by the formation of the so-called "ink-bottle" type pores in these samples. We speculate that such "ink-bottle" type pores arose likely from the location of Pd nanoparticles inside the cylindrical porous channels. The pore size distributions of

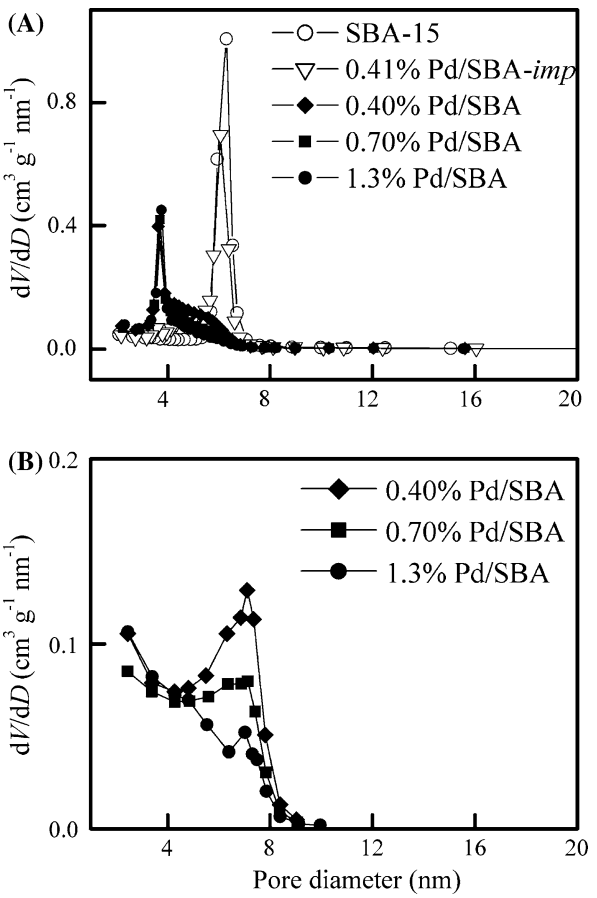

Fig. 5 Pore size distributions evaluated from N_2 adsorption–desorption isotherms by the BJH method. (**A**) Calculated from the desorption branch of the isotherms, (**B**) calculated from the adsorption branch of the isotherms

these Pd/SBA-15 samples calculated from the desorption branch by the BJH method (Fig. 5A) showed maxima at 3.6–3.8 nm, which was quite different from that for SBA-15 alone and for the 0.41 wt% Pd/SBA-15-*imp*. The same phenomenon was also reported for the SBA-15-encapsulated ZrO_2 nanoparticles [27], and it was proposed that, in this case, it was inappropriate to use the desorption branch of the isotherms to calculate the pore size distribution [28]. Instead, the calculation using the adsorption branch of isotherms could give more reasonable results [27]. The pore size distributions evaluated from the adsorption branches for the Pd/SBA-15 samples are shown in Fig. 5B, and the estimated average pore diameters for these samples are summarized in Table 2. The average pore diameters decreased with increasing the Pd content. Pore volume also decreased at the same. These results suggest that the Pd particles in the Pd/SBA-15 samples prepared by the adsorption method are located inside the mesoporous channels of SBA-15.

UV–vis spectroscopy was used to monitor the change of the state of palladium species after the adsorption and the subsequent calcination. As shown in Fig. 6A, the aqueous solution of $Pd(NH_3)_4Cl_2$ showed an absorption band at ~295 nm, which was ascribed to the d–d transition absorption of Pd species with 4-coordinated ammonia ligands in square-planar geometry [29, 30]. After the adsorption of the $[Pd(NH_3)_4]^{2+}$ into SBA-15 (0.70 wt% Pd/SBA-15 as an example in Fig. 6A), three new bands at 267, 340, and 420 nm appeared. These bands could be assigned to highly dispersed Pd(II) species coordinated with different numbers of NH_3 and OSi≡ ligands [29] such as $Pd(NH_3)_4^{2+}$, $Pd^{2+}(NH_3)_2(OSi\equiv)_2$, and $Pd^{2+}(OSi\equiv)_4$, which were probably formed via the interaction of the adsorbed Pd precursor with the ≡Si–O^- on the silica framework of SBA-15 in alkaline medium. After the calcination of the sample at 550 °C, the fine pattern disappeared, and a broad band at ~280 nm was observed. This broad band could be ascribed to highly dispersed Pd(II)O clusters or small PdO particles [31]. Thus, the highly dispersed Pd(II) species attached on silica wall of SBA-15 were transformed to small Pd(II)O clusters or PdO nanoparticles after calcination. This broad band was observed for the Pd/SBA-15 samples with other Pd contents (0.40 and 1.3 wt% as examples in Fig. 6B). A shoulder at ~470 nm, corresponding to relatively larger PdO particles, also became observable for the sample with a higher Pd content (1.3 wt%). On the other hand, for the Pd/SBA-15-*imp* sample after calcination, absorption bands at ~350 nm and ~470 nm were already clearly observed in addition to the band at ~280 nm in spite of the lower Pd content (0.41 wt%). Thus, for the 0.41 wt% Pd/SBA-15-*imp* sample after calcination, relatively larger PdO particles were already formed.

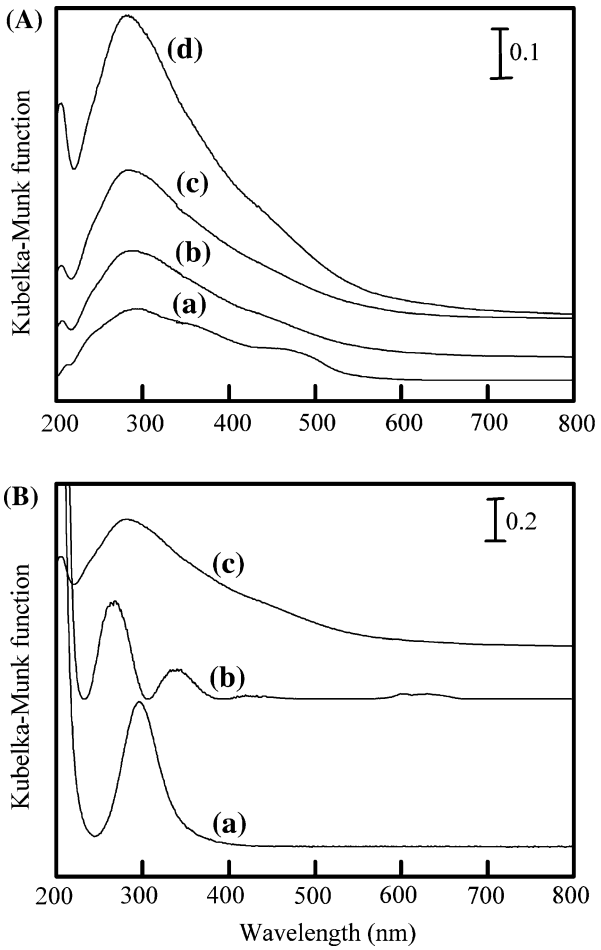

Fig. 6 UV–Vis spectra. (**A**): (a) $Pd(NH_3)_4Cl_2$ aqueous solution, (b) 0.70 wt% Pd/SBA-15 before calcination, (c) 0.70 wt% Pd/SBA-15 after calcination. (**B**): (a) 0.41 wt% Pd/SBA-15-*imp* after calcination, (b) 0.40 wt% Pd/SBA-15 after calcination, (c) 0.70 wt% Pd/SBA-15 after calcination, (d) 1.3 wt% Pd/SBA-15 after calcination

Figure 7 shows the typical TEM micrographs for the 0.40 wt% Pd/SBA-15 and the 0.41 wt% Pd/SBA-15-*imp* after reduction with H_2. The TEM images of SBA-15 alone were also shown in Fig. 7. SBA-15 alone exhibited regular hexagonal arrays of cylindrical mesoporous channels (Fig. 7A). Pd particles were clearly observed over SBA-15 for the Pd/SBA-15-*imp* sample (Fig. 7B), and the ordered structure of mesoporous channels was kept. The particle size distribution (Fig. 7B) derived from the TEM micrographs by counting ca. 100 particles showed that the size of Pd particles over this sample mainly ranged from 8 nm to 17 nm, and the mean size of the particles was calculated to be 10 nm. In other words, the sizes of Pd particles in the 0.41 wt% Pd/SBA-15-*imp* were significantly larger than the diameters of mesoporous channels. On the other hand, for the 0.41 wt% Pd/SBA-15 sample prepared by the adsorption method using SBA-15 with template removed by ethanol extraction as the support, the sizes of Pd

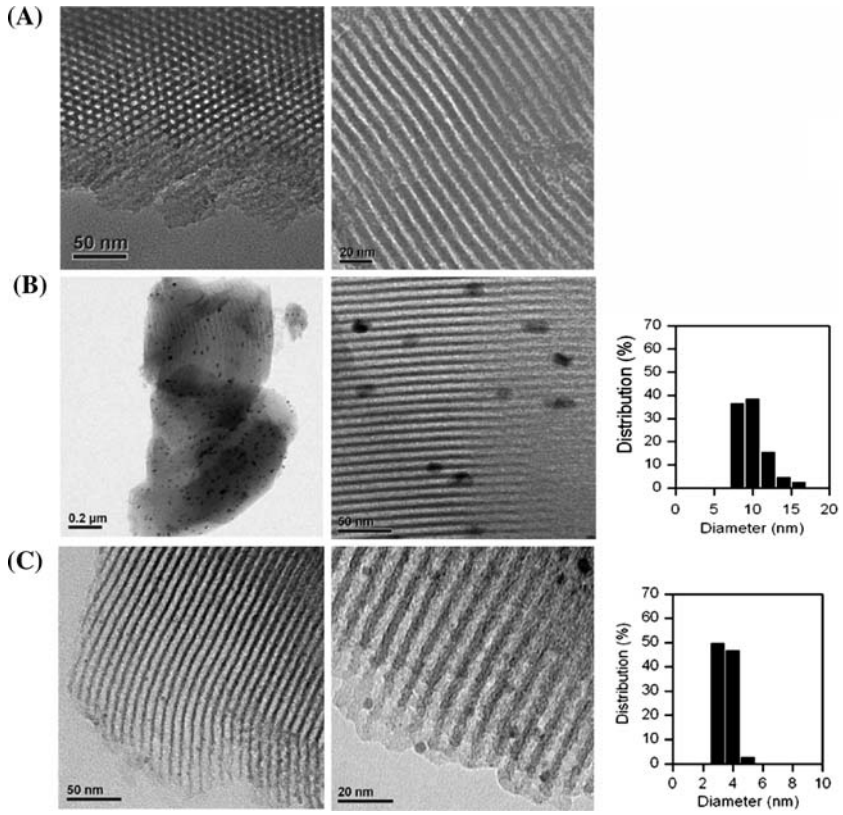

Fig. 7 TEM micrographs and Pd particle size distributions. (**A**) SBA-15, (**B**) 0.41 wt% Pd/SBA-15-*imp*, (**C**) 0.40 wt% Pd/SBA-15

particles were much smaller. TEM revealed that almost all of the Pd particles were located inside the mesoporous channels of SBA-15 (Fig. 7C). From the enlarged image (the middle of Fig. 7C), we could see that the sizes of most of the Pd particles were in the range of 3–4 nm, and the mean size of Pd particles was calculated to be 3.5 nm. TEM also confirmed that the ordered mesoporous structure was well sustained in this sample.

The typical TEM micrographs and the particle size distributions for the Pd/SBA-15 samples with other Pd contents are shown in Fig. 8. It is of interest to find that most of the Pd particles are located inside the mesoporous channels of SBA-15 even for the samples with a higher Pd content (2.2 wt%). The particle size distributions for these samples were quite narrow. The mean sizes of these samples calculated from the particle size distributions were ca. 3.3–3.9 nm as summarized in Table 3. Therefore, the adsorption method reported here is highly effective for the preparation of encapsulated Pd nanoparticles with very uniform particle sizes.

The dispersion of Pd, i.e., the fraction of surface Pd atoms in all of the Pd atoms in the sample was evaluated by CO chemisorption. The chemisorption stoichiometry of CO to the surface Pd atom was assumed to be 1. The results summarized also in Table 3 showed that the dispersion of Pd for the Pd/SBA-15 samples was significantly higher than that for the Pd/SBA-15-*imp*. This is in agreement with the TEM observation that the Pd particles in the former samples were much smaller than those in the latter sample. Moreover, consistent with the TEM observations, the Pd/SBA-15 samples with different Pd contents exhibited similar Pd dispersions.

3.2 Catalytic Behavior of the Pd/SBA-15 for Solvent-free Aerobic Oxidation of Alcohols

As reported previously, Pd nanoparticles were believed to be the active phase in many heterogeneous catalytic systems for the Pd-catalyzed aerobic oxidation of alcohols. The $Pd(OAc)_2$ immobilized on a bipyridylamide-modified SBA-15 was reported to be an efficient catalyst for the aerobic oxidation of alcohols, but a K_2CO_3 additive together with toluene solvent was required [32]. In this work, we examined the possibility of our Pd/SBA-15 catalysts for the aerobic oxidation of benzyl alcohol under solvent-free conditions in the absence of any additives.

As shown in Table 4, the 0.41 wt% Pd/SBA-15-*imp* (mean size of Pd, 10 nm) prepared by the impregnation method only showed a very low conversion of benzyl alcohol (entry 1). As compared with this sample, the Pd/SBA-15 series of samples prepared by the adsorption method using the SBA-15 with organic template removed by ethanol extraction exhibited significantly higher

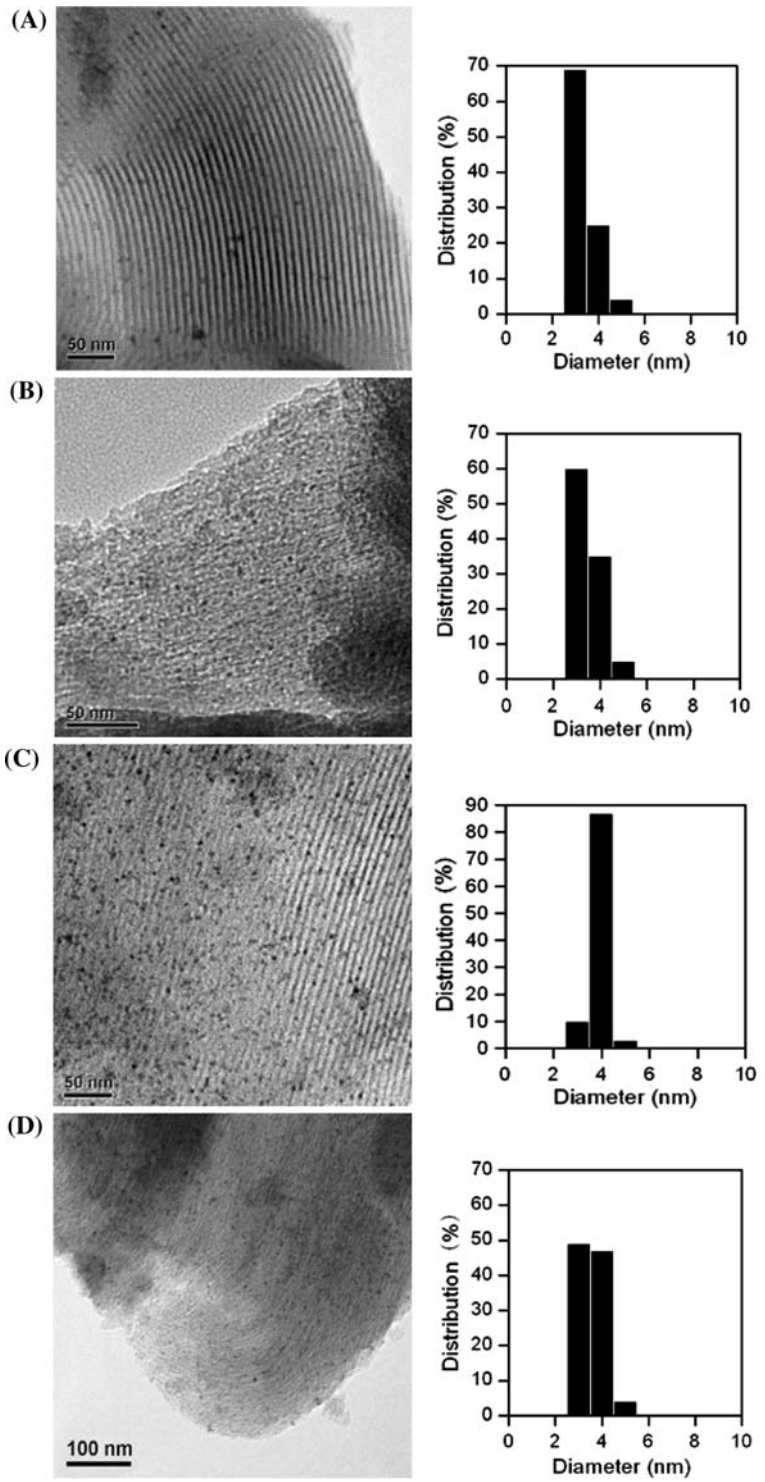

Fig. 8 TEM micrographs and Pd particle size distributions for the Pd/SBA-15 samples with different Pd contents. (**A**) 0.70 wt% Pd/SBA-15, (**B**) 1.3 wt% Pd/SBA-15, (**C**) 1.6 wt% Pd/SBA-15, (**D**) 2.2 wt% Pd/SBA-15

conversions of benzyl alcohol (entries 3–6). The turnover frequency (TOF) calculated by the conversion of benzyl alcohol per surface Pd atom over the 0.40 wt% Pd/SBA-15 (mean size of Pd, 3.5 nm) was also significantly higher than that over the 0.41 wt% Pd/SBA-15-*imp*. Moreover, the present 0.40 wt% Pd/SBA-15 was more active than the 0.32 wt% Pd/Al_2O_3 (mean size of Pd, $\sim$5 nm) reported previously [7] for the oxidation of benzyl alcohol under the reaction conditions in Table 4 (entry 2). This confirms that smaller Pd particles prepared in SBA-15 were more active toward alcohol oxidation than the larger Pd particles. The feature that the present Pd/SBA-15 catalyst could be

Table 3 Mean size and dispersion of Pd particles in Pd/SBA-15

Sample	Mean size of Pd[a] (nm)	Pd dispersion[b]
0.41 wt% Pd/SBA-15-*imp*	10	0.14
0.40 wt% Pd/SBA-15	3.5	0.24
0.70 wt% Pd/SBA-15	3.3	0.27
1.3 wt% Pd/SBA-15	3.5	0.26
1.6 wt% Pd/SBA-15	3.9	n.d.
2.2 wt% Pd/SBA-15	3.6	0.26

[a] Obtained from TEM observations

[b] Evaluated from CO chemisorption by assuming the chemisorption stoichiometry of CO to surface Pd atom of 1

operated in the absence of a base additive is similar to those observed for many other heterogeneous catalysts with Pd nanoparticles as the active phase [4–7, 33]. Further comparisons with other heterogeneous catalysts suggest that the present Pd/SBA-15 catalyst possesses higher activity for the oxidation of benzyl alcohol. For examples, Au–Pd/TiO_2 and Au/zeolite-beta catalysts exhibited TOFs of 6,190 and 378 h^{-1}, respectively, for the solvent-free aerobic oxidation of benzyl alcohol at 100 °C [34, 35]. Many other catalysts such as 0.3% Pd/hydroxyapatite and 1.4% Ru/Al_2O_3 gave TOFs less than 500 h^{-1} for the same reaction in the presence of an organic solvent [33].

For the Pd/SBA-15 series of catalysts, the conversion of benzyl alcohol increased with increasing the Pd content up to 1.3 wt%, and further increases in the Pd content decreased the conversion of benzyl alcohol. The TOF based on surface Pd atoms decreased monotonically with increasing the Pd content. We speculate that the relatively larger pore size of SBA-15 can accelerate the diffusion of alcohol molecules and thus is beneficial to the reaction. Because almost all the Pd nanoparticles with diameters of 3–4 nm were encapsulated inside the mesoporous channels with diameters of ca. 5–6 nm in the Pd/SBA-15 catalysts, the higher Pd content would cause larger diffusion resistance, and thus, caused the lower intrinsic activity.

Table 4 Comparison of catalytic properties of different catalysts for the aerobic oxidation of benzyl alcohol under solvent-free conditions[a]

Entry	Catalyst	Conv. (%)	Benzaldehyde select.[b] (%)	TOF[c] (h^{-1})
1	0.41 wt% Pd/SBA-15-*imp*	10	100	489
2	0.32 wt% Pd/Al_2O_3	12	97	3150
3	0.40 wt% Pd/SBA-15	75	80	10500
4	0.70 wt% Pd/SBA-15	88	85	6170
5	1.3 wt% Pd/SBA-15	96	80	3690
6	2.2 wt% Pd/SBA-15	85	81	1960
7[d]	1.3 wt% Pd/SBA-15	8.1	55	214

[a] Reaction conditions: catalyst, 0.1 g; benzyl alcohol, 48.5 mmol; O_2 flow, 3 mL min^{-1}; reaction temperature, 80 °C; time, 4 h

[b] The remaining product is toluene

[c] Calculated by the moles of benzyl alcohol per mole of surface Pd per hour

[d] Using N_2 (3 mL min^{-1}) instead of O_2

The selectivity for benzaldehyde was ca. 80–90%, and the remaining product was toluene over our Pd/SBA-15 samples with different Pd contents. It is of interest to note that such a selectivity pattern is quite similar to that reported for the aerobic oxidation of benzyl alcohol over a $Pd_{561}phen_{60}(OAc)_{180}$ (phen = 1,10-phenanthroline) giant cluster (Pd metal, 2–3 nm, total ~5 nm) [36]. It has been proposed that the disproportionation of benzyl alcohol to benzaldehyde and toluene (Eq. 4) occurred in parallel to the selective oxidation of benzyl alcohol to benzyladehyde (Eq. 5) [36]. Over our catalyst, we found that the use of N_2 instead of O_2 for conversion of benzyl alcohol caused the formation of benzaldehyde and toluene with a ratio of 55/45 (Table 4). This result indicates that the disproportionation of benzyl alcohol also occurred to some extent in our case.

$$2PhCH_2OH \rightarrow PhCHO + PhCH_3 + H_2O \quad (4)$$

$$PhCH_2OH \rightarrow 1/2O_2 + PhCHO + H_2O \quad (5)$$

We have examined the recycling uses of the 0.70 wt% Pd/SBA-15 catalyst for the aerobic oxidation of benzyl alcohol under solvent-free conditions. The result shown in Fig. 9 suggests that benzyl alcohol conversion only decreased very slightly after repeated uses for five times.

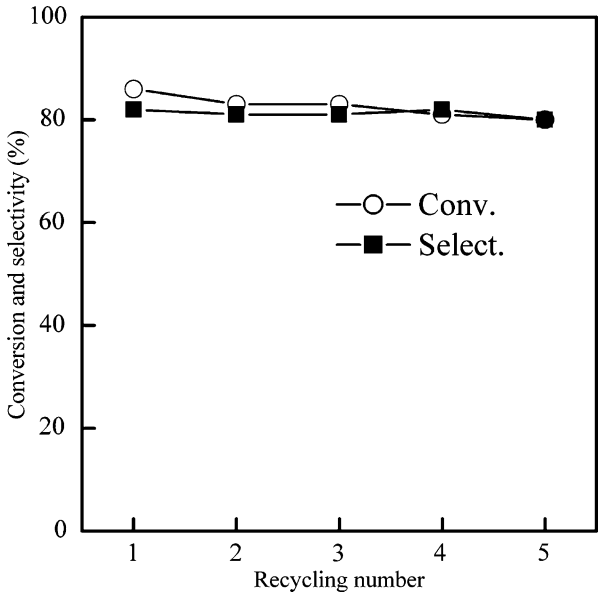

Fig. 9 Recycling uses of the 0.70 wt% Pd/SBA-15 for the aerobic oxidation of benzyl alcohol under solvent-free conditions. Reaction conditions: catalyst, 0.1 g; benzyl alcohol, 48.5 mmol; O_2 flow, 3 mL min^{-1}; temperature, 80 °C; time, 4 h

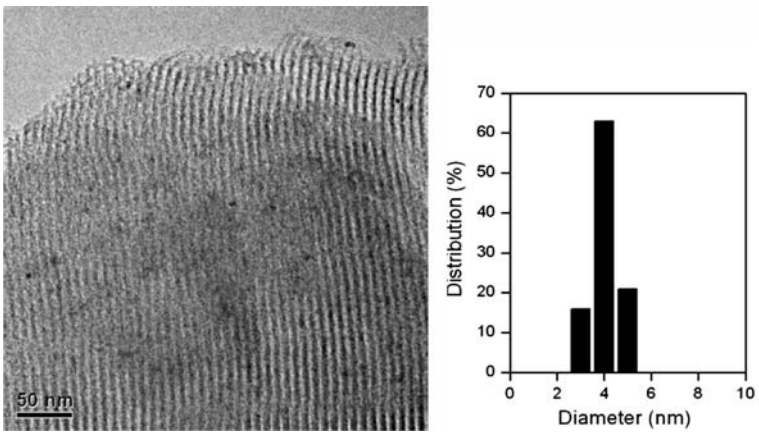

Fig. 10 TEM micrograph and Pd particle size distribution for the 0.70 wt% Pd/SBA-15 after recycling uses for five times. The reaction conditions are shown in Fig. 9

Table 5 Catalytic performances of the 0.70 wt% Pd/SBA-15 catalyst for the aerobic oxidation of various alcohols under solvent-free conditions[a]

Entry	Alcohol	Time (h)	Temp. (°C)	Conv. (%)	Aldehyde/ketone select. (%)
1[b]	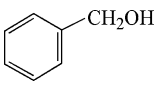	4	80	88	85
2[c]	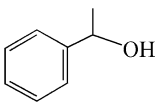	4	150	90	94
3[d]	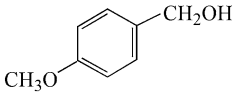	24	100	90	88
4	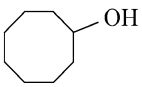	48	100	30	100
5	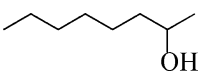	48	150	91	100
7[e]	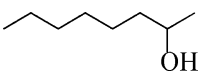	96	150	96	100

[a] Reaction conditions: substrate, 50 mmol; catalyst, 0.1 g; O_2 flow, 3 mL min^{-1}

[b] The by-product was toluene

[c] The by-product was ethylbenzene

[d] The by-product was 4-methoxyl toluene

[e] Catalyst, 0.32 wt% Pd/Al_2O_3 [7]

We have also carried out TEM measurements for the 0.70 wt% Pd/SBA-15 after the repeated uses. The typical TEM image and the particle size distribution are shown in Fig. 10. The TEM result reveals that the mesoporous structure of SBA-15 is still maintained after the repeated uses for five times. The mean size of Pd particles calculated from the size distribution was 4.0 nm, which was only slightly larger than that of the fresh catalyst.

Table 5 shows the catalytic performances of the 0.70 wt% Pd/SBA-15 catalyst for the solvent-free aerobic oxidation of other alcohols. The present catalyst could catalyze the oxidations of not only benzylic alcohols but also nonactivated alcohols such as 2-octanol under solvent-free conditions.

4 Conclusions

We succeeded in preparing SBA-15-encapsulated palladium nanoparticles by a simple adsorption method using

the SBA-15 with organic template removed by ethanol extraction for the adsorption of cationic palladium precursor in alkaline solution. The pH of the palladium precursor solution was a critical factor for adsorption. By regulating the pH of the solution and the concentration of palladium precursor, we could incorporate $\sim$4 wt% of palladium to SBA-15 by keeping the ordered mesoporous structure. The palladium nanoparticles were located inside the mesoporous channels of SBA-15 and were quite uniform in size. The mean diameters of the palladium nanoparticles were 3–4 nm. On the other hand, the conventional impregnation of the calcined SBA-15 with the same cationic palladium precursor formed remarkably larger Pd particles. The SBA-15-encapsulated palladium nanoparticles with uniform sizes of 3–4 nm could catalyze the solvent-free aerobic oxidation of benzyl alcohol efficiently. These palladium nanoparticles showed significantly higher activity than those prepared over the calcined SBA-15 by the impregnation. The selectivity pattern of our Pd/SBA-15 catalyst in the oxidation of benzyl alcohol was similar to that reported for a giant Pd nanocluster with size of Pd of 2–3 nm.

Acknowledgments This work was supported by the National Natural Science Foundation of China (20625310 and 20433030), the National Basic Research Program of China (2003CB615803 and 2005CB221408), the Key Scientific Project of Fujian Province of China (No. 2005HZ01-3), and the Program for New Century Excellent Talents in Fujian province (to Q.Z.).

References

1. Mandal S, Roy D, Chaudhari RV, Sastry M (2004) Chem Mater 16:3714
2. Phan NTS, Sluys MVD, Jones CW (2006) Adv Synth Catal 348:609
3. Astruc D (2007) Inorg Chem 46:1884
4. Mori K, Hara T, Mizugaki T, Ebitani K, Kaneda K (2004) J Am Chem Soc 126:10657
5. Pillai UR, Sahle-Demessie E (2004) Green Chem 6:161
6. Kwon MS, Kim N, Park CM, Lee JS, Kang KY, Park J (2005) Org Lett 7:1077
7. Wu H, Zhang Q, Wang Y (2005) Adv Synth Catal 347:1356
8. Corma A (1997) Chem Rev 97:2373
9. Ying JY, Mehnert CP, Wong MS (1999) Angew Chem Int Ed 38:56
10. Shi J, Hua Z, Zhang L (2004) J Mater Chem 14:795
11. Taguchi A, Schüth F (2005) Microporous Mesoporous Mater 77:1
12. Zhu SM, Zhou HS, Hibino M, Honma I (2003) J Mater Chem 23:1115
13. Kónya Z, Molnar E, Tasi G, Niesz K, Somorjai GA, Kiricsi I (2007) Catal Lett 113:19
14. Suvanto S, Hukkamäki J, Pakkanen TT, Pakkanen TA (2000) Langmuir 16:4109
15. Kónya Z, Puntes VF, Kiricsi I, Zhu J, Alivisatos P, Somorjai GA (2002) Catal Lett 81:137
16. Song H, Rioux RM, Hoefelmeyer JD, Komor R, Niesz K, Grass M, Yang P, Somorjai GA (2006) J Am Chem Soc 128:3027
17. Jiang YX, Ding N, Sun SG (2004) J Electroanal Chem 563:15
18. Lee SS, Park HI, Park BK, Byeon SH (2006) Mater Sci Eng B 135:20
19. Lee KB, Lee SM, Cheon J (2003) Adv Mater 13:517
20. Yuranov I, Moeckli P, Suvorova E, Buffat P, Kiwi-Minsker L, Renken A (2003) J Mol Catal A 192:239
21. Yuranov I, Kiwi-Minsker L, Buffat P, Renken A (2004) Chem Mater 16:760
22. Schwarz JA, Contescu C, Contescu A (1995) Chem Rev 95:477
23. Zhao D, Huo Q, Feng J, Chmelka BF, Stucky GD (1998) J Am Chem Soc 120:6024
24. Mercier L, Pinnavaia TJ (1998) Environ Sci Technol 32:2749
25. Bourikas K, Kordulis C, Lycourghiotis A (2005) Environ Sci Technol 39:4100
26. Schuth F, Wingen A, Sauer J (2001) Microporous Mesoporous Mater 44–45:465
27. Vradman L, Landau MV, Kantorovich D, Koltypin Y, Gedanken A (2005) Micropor Mesopor Mater 79:307
28. Rouquerol F, Rouquerol J, Sing KSW (2002) Handbook of porous solides. Wiley-VCH, Weinheim
29. Zhang Z, Sachtler WMH, Chen H (1990) Zeolite 10:784
30. Bonivardi AL, Baltanás MA (1990) J Catal 125:243
31. Pestryakov AN, Lunin VV, Fuentes S, Bogdanchikova N, Barrera A (2003) Chem Phys Lett 367:102
32. Karimi B, Abedi S, Clark JH, Budarin V (2006) Angew Chem Int Ed 45:4776
33. Mallat T, Baiker A (2004) Chem Rev 104:3037
34. Enache DI, Edwards JK, Landon P, Solsona-Espriu B, Carley AF, Herzing AA, Watanabe M, Kiely CJ, Knight DW, Hutchings GJ (2006) Science 311:362
35. Li G, Enache DI, Edwards J, Carley AF, Knight DW, Hutchings GJ (2006) Catal Lett 110:7
36. Kovtun G, Kameneva T, Hladyi S, Staechevsky M, Pazdersky Y, Stolarov I, Vargaftik M, Moiseev I (2002) Adv Synth Catal 344:957